Hindawi
International Journal of Mathematics and Mathematical Sciences
Volume 2023, Article ID 6282130, 14 pages
https://doi.org/10.1155/2023/6282130

Research Article

Tangent Hyperbolic Fluid Flow under Condition of Divergent Channel in the Presence of Porous Medium with Suction/Blowing and Heat Source: Emergence of the Boundary Layer

Sushila Choudhary,[1] **Prasun Choudhary**,[1] **and Balachandra Pattanaik**[2,3]

[1]*Department of Mathematics, University of Rajasthan, Jaipur 302004, India*
[2]*College of Engineering and Technology, Wollega University, Nekemte, Ethiopia*
[3]*Saveetha School of Engineering, Saveetha Institute of Medical and Technical Sciences, Chennai, India*

Correspondence should be addressed to Prasun Choudhary; prasun.iimet@gmail.com and Balachandra Pattanaik; balapk1971@gmail.com

Received 16 March 2023; Revised 11 April 2023; Accepted 24 June 2023; Published 30 June 2023

Academic Editor: Saranya Shekar

A boundary layer's appearance in a diverging permeable channel for a non-Newtonian hyperbolic tangent fluid with heat transfer in the availability of a heat source and suction or injection is investigated. By controlling backflow, nonlinearly associated ODEs are derived from flow-regulating PDEs, and the restrictions under which the formation of a boundary layer for tangent hyperbolic fluid emerges are investigated. It is obtained that mass suction is an expression of the Hartmann number, porosity parameter, and power law index parameter, and when it surpasses a specific quantity, flow within a boundary layer is conceivable. "Bvp4c," a MATLAB solver, is used to obtain numerical solutions of flow problem, and for validation of results obtained via Bvp4c, a comparison is made with the methodology of the Runge–Kutta fourth order. As the Weissenberg number enhances, flow in a boundary layer decreases. Furthermore, radiation and heat source parameters have a significant influence on the overall temperature pattern, and as the findings, the thermal boundary layer enhances.

1. Introduction

Several polymers conform to the qualities of non-Newtonian fluids. Lubricants, detergents, paints, molten polymers, and foods are all instances of non-Newtonian fluids which does not obey Newton's viscosity law. The connection between shear stress and velocity for such fluids does not maintain a linear relationship, and variations in their viscosities are seen differentially with respect to shear stress. On the basis of this approach, the governing flow relating to these fluids is exceedingly complex, and classical visualizations of Newtonian fluids are incapable of approximating and predicting the behaviour of these non-Newtonian fluids. As a consequence, several constitutive equations aid in describing the movements of fluids (non-Newtonian) during flow. One of them is tangent hyperbolic fluid, which is significant because this model accurately anticipates the effect of shear thinning. The initial presentation of the hyperbolic tangent flow model was made by Pop and Ingham [1]. Brujan [2] discusses the numerous non-Newtonian fluid modeling of constituent elements, which identify the diverse flow features of commercial fluids such as whipped cream, ketchup, and nail polish. Akbar et al. [3] outlined a mathematical approach for the movement of a tangent hyperbolic fluid in a magnetohydrodynamic boundary layer approaching an enlarging sheet. Prasad et al. [4] demonstrated heat transmission and free convection of an isothermal spherical context, a hyperbolic tangent fluid that is not Newtonian with some slippage. Due to the vast industrial uses of tangent hyperbolic fluid, numerous authors, such as Ramachandra Prasad et al. [5]; Abbas et al. [6]; and Farooq et al. [7], have written about it. Sindhu and Gireesha [8] and Ahmad et al. [9] have

investigated this phenomenon from multiple perspectives. Jat and Sharma [10] investigated heat transfer simulation and hyperbolic tangent nanofluid unsteady MHD flow over an angled stretched sheet. The efficiency of energy systems was explored by Ali et al. [11] in their discussion of bioconvective implications of unsteady slip flow past a hyperbolic tangent nanoliquid with surface heating. Quantitative research into the transportation of tangent hyperbolic hybrid nanofluid through the Riga wedge was mentioned by Yahya et al. [12].

Due to the absence of clarity in the creation of layer structure at the boundary nearby the two walls of the channels, the flow of a viscous liquid that cannot be compressed along a diverging channel is a significant challenge in fluid dynamics. Several backflow areas are produced above a certain Reynolds number value, and viscosity's consequences on fluid behaviour are strong throughout the whole channel. Jeffery [13] and Hamel [14] were the first to explore converging and diverging channels. In their research, walls with channels were considered to be immobile, and flow was attributed to the persistence of fluid mass source or sink at the intersection of a combination of channel walls. Haines et al. [15] subsequently provided a solution based on similarities identified by Jeffery and Hamel and its application to flow in a channel that is diverging. Bhattacharyya and Layek [16] demonstrated dilatant fluid movement in a diverging channel with MHD boundary layers under suction or blowing. Additionally, Layek et al. [17] studied magnetohydrodynamic (MHD) flow with consistent suction or blowing in a diverging channel. Erdinç [18] examined numerically the flow and heat transfer in dealing with divergent and convergent channels. Recently, Iyyappan and Singh [19] and Banerjee et al. [20] have conducted research on diverging channel flow. Siddique et al. [21] analysed natural convection in nanofluid flow through a conduit with a source/sink effect.

In recent decades, the mechanism of transfer of heat in the context of thermal radiation has also attracted the attention of scholars in innovative thermal techniques. Thermal radiation findings are especially important in the creation of reliable services, nuclear plants, gas engines, various spacecraft propulsion instruments, rockets, and satellites, as well as in the analysis of thermal influences in the context of high-temperature flow structures. Thermal radiation performed a major role in modulating the phase of heat transport in the polymer sectors. In addition, it is important to keep in mind that linear radiation controls the heat transfer rate. By linearizing the radiative heat, the Rosseland approximation is responsible for the influence of thermal radiation. In recent years, the following researches are performed in this field. A thermal assessment of a radiative nanofluid across a stretching/shrinking cylinder with viscous dissipation was published by Alqahtani et al. [22]. In the context of radiative stagnation point flow of nanofluid with cross-diffusion and viscous dissipation, Qaiser et al. [23] illustrated the relevance of entropy optimization and activation energy. Using a computational technique, Khan et al. [24] explored the movement of mass and energy in a hybrid nanofluid flowing across an extended cylinder containing a magnetic dipole. Nonlinear radiative nanofluidic hydrothermal unsteady bidirectional transport with thermal/mass convection issues was researched by Faisal et al. [25]. The effects of thermal radiation and viscosity dissipation on the flow of water- and kerosene-based carbon nanotubes through a heated Riga sheet were studied by Prabakaran et al. [26].

It is generally recognized that mass suction/blowing introduced into an existing flow field has the potential to alter the entire flow dynamics and the entire heat transfer process, as it has the ability to disrupt the mainstream flow. Together with this, suction/blowing has a substantial effect on a variety of engineering operations, particularly those involving channel flow or heat transfer. Contrary to popular perception, diffuser flow with divergence can be divided into an inviscid main flow and a thick boundary layer on two walls at high Reynolds numbers. If a significant quantity of fluid mass suction is applied via a porous channel with a highly separating flow with a greater Reynolds number, then boundary layer structure will be observed. Rundora and Makinde [27] investigated suction and injection's influence on the motion of fluid that does not follow the Newtonian model inside a permeable medium channel with a state of convection at the boundary. Mansur et al. [28] characterized a nanofluid's stagnation point flow in magnetohydrodynamics (MHD) over a contracting/expanding sheet under suction. Using the homotopy analysis method, Animasaun et al. [29] investigated modification in thermo-physical characteristics of a Casson fluid along an exponentially expanded sheet with suction and exponentially decreasing emission of heat. Using an analytic approach, Hussanan et al. [30] provided a suction or injection flow problem of a viscoelastic Casson fluid across a stretched surface under the action of dissipation of viscosity. Li et al. [31] analysed the flow of liquid food according to the power law through an irregular conduit with nonuniform suction/injection. Abdal et al. [32] researched the solution availability of MHD Casson nanofluid transport across a stretching cylinder through porous media as well as the evaluation of a priori bounds. Both analytical and computational examinations of MHD movement in a convergent/divergent channel subjected to boundary stresses were conducted by Asghar et al. [33].

According to the aforementioned survey, hardly attempting has been made for the divergent channel flow assessment of the magnetized tangent hyperbolic fluid through a porous medium taking suction/blowing into consideration. The novelty of the present study includes the following:

(i) In the appearance of suction/blowing, tangent hyperbolic fluid flows in a divergent channel

(ii) Condition of a boundary layer existence, so that separation in divergent channel flow can be prevented

(iii) The heat transfer feature with the involvement of a heat source and radiation

Utilizing the MATLAB Bvp4c code, the numerical results are obtained. Many parameters and their graphical trends in relation to velocity, temperature, skin friction drag coefficient, and heat transfer rate are inspected and elaborated appropriately.

We will be capable to respond the relevant questions at the conclusion of this analysis:

(i) What is the precise amount of mass suction needed for flow within the boundary layer?

(ii) How do the representative parameters of the hyperbolic tangent fluid influence the velocity and temperature fields?

(iii) What influence do radiation and heat source factors have on heat transfer rate?

(iv) How does the skin friction coefficient correlate with the various flow parameters?

2. Flow Formulation

Consider the time-independent 2D flow of an electrically conducting tangent hyperbolic fluid in a channel that is divergent. Walls of the channel are assumed to be immovable and porous, by which mass suction or blowing is placed. The flow close to only one wall of the channel is shown below because the other channel wall should have an identical flow configuration. The x-axis is situated along the considered wall, and the y-axis is perpendicular to the x-axis, with the connection of two-channel walls serving as the origin.

The fundamental equations for the 2D flow of an incompressible fluid are the conservation of mass, linear momentum, and energy. These equations are formulated in the context of body forces as described as follows (Bansal [34]):

$$\operatorname{div}\vec{V} = 0, \tag{1}$$

$$\rho\frac{D\vec{V}}{Dt} \equiv \rho\vec{F} + \operatorname{div}\overleftrightarrow{M}, \tag{2}$$

$$\rho c_p\frac{DT}{Dt} \equiv Q^* + \kappa\left\{\frac{\partial}{\partial x}\left(\frac{\partial T}{\partial x}\right) + \frac{\partial}{\partial y}\left(\frac{\partial T}{\partial y}\right)\right\} + \varphi, \tag{3}$$

where $D/Dt = \partial/\partial t + u\partial/\partial x + v\partial/\partial y$ (total time derivative), $\vec{V} = (u, v)$ is velocity vector, and $\varphi = \overleftrightarrow{\tau}.\nabla\vec{V}$ is viscous dissipation term.

2.1. Tangent Hyperbolic Fluid Model. The Cauchy stress tensor for tangent hyperbolic fluid is as follows:

$$\overleftrightarrow{M} = -p\overleftrightarrow{I} + \overleftrightarrow{\tau}. \tag{4}$$

In the model of tangent hyperbolic fluid (Patil and Raju [35]), the extra stress tensor (τ) expression is denoted as follows:

$$\overleftrightarrow{\tau} = \left[\mu_\infty + (\mu_0 + \mu_\infty)\tanh\left(\Gamma\dot{\gamma}\right)^n\right]A_1, \tag{5}$$

where $A_1 = \operatorname{grad}\vec{V} + (\operatorname{grad}\vec{V})^T$ is first Rivlin–Ericksen tensor, and $\dot{\gamma}$ is classified as

$$\begin{aligned}\dot{\gamma} &= \sqrt{\frac{1}{2}\sum_i\sum_j \dot{\gamma}_{ij}\dot{\gamma}_{ji}}\\ &= \sqrt{\frac{1}{2}\operatorname{trace}\left(A_1\right)^2}.\end{aligned} \tag{6}$$

Here, we assume $\mu_\infty = 0$ because the explanation of the infinity shear rate viscosity phenomenon is not practicable, and $\Gamma\dot{\gamma} < 1$, as we are researching about hyperbolic tangent fluid, which has shear thinning features. Thus, the required form of equation (5) is written by

$$\begin{aligned}\overleftrightarrow{\tau} &= \mu_0\left(\Gamma\dot{\gamma}\right)^n A_1\\ &= \mu_0\left[1 + \Gamma\dot{\gamma} - 1\right]^n A_1 \approx \mu_0\left[1 + n(\Gamma\dot{\gamma} - 1)\right]A_1.\end{aligned} \tag{7}$$

2.2. Continuity Equation. For steady two-dimensional flow, the continuity equation can be expressed as follows:

$$\frac{\partial u}{\partial x} + \frac{\partial v}{\partial y} = 0. \tag{8}$$

2.3. Momentum Equation. Considering the impact of magnetic field and porous medium and using the resulting form of the specified model (Patil and Raju [35]) in equation (2), we obtain

$$\begin{aligned}u\frac{\partial u}{\partial x} + v\frac{\partial u}{\partial y} = &-\frac{1}{\rho}\frac{\partial p}{\partial x} + \upsilon\left((1-n)\frac{\partial^2 u}{\partial y^2} + n\sqrt{2}\,\Gamma\frac{\partial u}{\partial y}\frac{\partial^2 u}{\partial y^2}\right)\\ &-\frac{\upsilon}{k_p}u - \frac{\sigma {B_0}^2}{\rho}u,\end{aligned} \tag{9}$$

$$-\frac{1}{\rho}\frac{\partial p}{\partial y} = 0, \tag{10}$$

where the components standing for velocity in the x- and y-directions are u and v, correspondingly, and kinematic fluid density and viscosity, respectively, are υ and ρ.

For flow components, boundary conditions are

$$\left.\begin{aligned}&u = 0, v = -v_w(x) \quad at\ y = 0;\\ &u \longrightarrow U(x) \quad for\ x > 0 \quad as \quad y \longrightarrow \infty.\end{aligned}\right\} \tag{11}$$

The free-stream variable velocity is stated as follows:

$$\begin{aligned}U(x) &= \frac{Q_1}{\alpha x}\\ &= \frac{U_0 L}{x}\ (U_0 > 0),\end{aligned} \tag{12}$$

where α is the channel angle, $Q_1 > 0$ is a fixed constant, and U_0 and L are the specific velocity and length, respectively.

The implemented suction/blowing velocity, $v_w(x)$ through the permeable walls of the diverging channel, is given by

$$v_w(x) = \frac{S^*\sqrt{Q_1 v}}{x\sqrt{\alpha}}, \tag{13}$$

where S^* stands for the mass suction or blowing parameter, and $S^* < 0$ and $S^* > 0$ relate to both mass blowing and mass suction, correspondingly. Figure 1 depicts a portrait of the flow zone of a diverging channel as well as additional information.

It is clear from the sequential assessment of the preceding momentum-based equations (there are two of them) that $\|\partial p/\partial y\| \ll \|\partial p/\partial x\|$. As a result, for the boundary layer, the pressure p is just an expression of x to the initial approximation. Using the free-stream zone (inviscid flow region), pressure gradient $\partial p/\partial x$ can be calculated from equation (9).

$$-\frac{1}{\rho}\frac{\partial p}{\partial x} = U\frac{dU}{dx} + \frac{v}{k_p}U + \frac{\sigma {B_0}^2}{\rho}U. \tag{14}$$

By removing $\partial p/\partial x$ from equations (9) and (14), we achieve

$$u\frac{\partial u}{\partial x} + v\frac{\partial u}{\partial y} = U\frac{dU}{dx} + v\left((1-n)\frac{\partial^2 u}{\partial y^2} + n\sqrt{2}\,\Gamma\frac{\partial u}{\partial y}\frac{\partial^2 u}{\partial y^2}\right) + \frac{v}{k_p}(U-u) + \frac{\sigma {B_0}^2}{\rho}(U-u). \tag{15}$$

Equations (1) and (12) admit the following similarity solution (Banerjee et al. [20]):

$$u = \frac{Q_1}{\alpha x}f(\eta) \text{ and } v = \sqrt{\frac{Q_1 v}{\alpha}}\left[\frac{\eta f(\eta) - S^*}{x}\right], \tag{16}$$

where $\eta = y/x\sqrt{Q_1/\alpha v}$ is a similarity variable.

Equation (4) for continuity is naturally fulfilled, and equation (15) is converted to the self-similar equation shown as follows:

$$(1-n)f'' - \left(1-f^2\right) + S^* f' + n\lambda_x f' f'' + (Ha+\delta)(1-f) = 0. \tag{17}$$

with

$$\left.\begin{aligned} f(\eta) &= 0 \quad \text{at } \eta = 0; \\ f(\eta) &= 1 \quad \text{as } \eta \longrightarrow \infty. \end{aligned}\right\} \tag{18}$$

2.4. Possibility of Boundary Layer Flow and Separation Control. The steady state of the boundary layer tangent hyperbolic fluid via a conduit/channel which diverges is not possible due to an instance of backflow; however, backflow may be avoided, and separation of boundary layers can be regulated, which is extremely significant. Magnitude $f'(\eta) = Z$ (assume) is proportional to the change of rate in velocity within the flow zone of the boundary layer; i.e., $(\partial u/\partial y)$. Now, as the quantity $\partial u/\partial y$ steadily decreases throughout the boundary layer and approaches zero at the boundary point, it is clear that Z is an expression of η that lowers

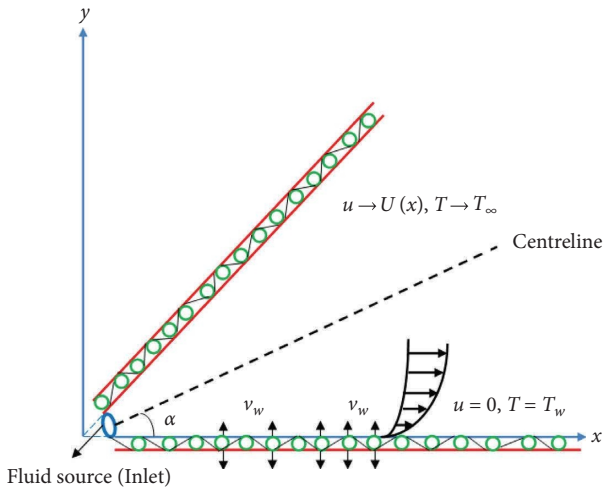

Figure 1: Fluid model.

regularly. Thus, $Z'(\eta) < 0$ on the inner of the boundary layer and $Z \longrightarrow 0$ as $\eta \longrightarrow \infty$. As a result, as η transforms from 0 (towards the wall of channel) to ∞ (in free-stream), $f(\eta)$ expands from 0 (at the wall of channel) to 1 (at the boundary point of the boundary layer); hence, $f'(\eta) > 0$. As a result, $dZ/df = (dZ/d\eta)/(df/d\eta)$ is negative throughout the region of a boundary layer, and $Z \longrightarrow 0$ as $f \longrightarrow 1$ (Bhattacharyya and Layek [16]).

Self-similar equation (17) is written by replacing $f''(\eta) = ZdZ/df$.

$$\frac{dZ}{df} = \frac{\left(1-f^2\right) - S^* Z + (Ha+\delta)(f-1)}{(1-n)Z + n\lambda_x Z^2}. \tag{19}$$

Imposing a limit as $f \longrightarrow 1$ and also $Z \longrightarrow 0$ as $f \longrightarrow 1$, equation (19) changes to

$$\lim_{f\longrightarrow 1}\frac{dZ}{df} = \lim_{f\longrightarrow 1}\frac{\left(1-f^2\right) - S^* Z + (\mathrm{Ha}+\delta)(f-1)}{(1-n)Z + n\lambda_x Z^2}. \tag{20}$$

The R.H.S. (right hand side) limit is undefined; hence, it is converted to

$$\lim_{\mathrm{f}\longrightarrow 1}\mathrm{dZ/df} = \lim_{\mathrm{f}\longrightarrow 1} -2\mathrm{f} - \mathrm{S}^*\mathrm{dZ/df} + (\mathrm{Ha}+\delta)/(1-\mathrm{n})\mathrm{dZ/df} + 2\mathrm{n}\lambda_x \mathrm{ZdZ/df}, \tag{21}$$

$$\text{Let } \lim_{f\longrightarrow 1}\frac{dZ}{df} = F. \tag{22}$$

Using equation (22) in equation (21), we get

$$F = \frac{-2(1) - S^* F + (\mathrm{Ha}+\delta)}{(1-n)F + 2n\lambda_x \times 0 \times F} = \frac{-2 - S^* F + (\mathrm{Ha}+\delta)}{(1-n)F}. \tag{23}$$

Furthermore, by solving equation (23), a quadratic equation in F is derived, which offers two values of F.

$$F = \frac{-S^* \pm \sqrt{(S^*)^2 - 4[2-(Ha+\delta)](1-n)}}{2(1-n)}. \tag{24}$$

If a boundary layer structure is to form near the two channel walls, the value of F must be negative over the whole boundary layer. Therefore, it is obvious that if the parameter $S^* \geq 2\sqrt{[2-(\mathrm{Ha}+\delta)](1-n)}$, then the measurement of F is negative for one of the two values. As a result, the divergent channel boundary layer experiences tangent hyperbolic fluid flow, and separation is kept under control by blocking backflow only when mass suction reaches a certain level. When any given tangent hyperbolic fluid (fixed value of n) is investigated, there is obviously neither a mass suction/blowing situation nor mass blowing with a boundary layer structure exists. It is worth noting that as $n = 0$, tangent hyperbolic fluid transforms into Newtonian fluid, and it is only when $S^* \geq 2\sqrt{2-(\mathrm{Ha}+\delta)}$, then boundary layer flow is commenced.

2.5. Thermal Analysis. Considering the impact of radiation, heat generation, and dissipation, the temperature equation (3) for tangent hyperbolic fluid (Patil and Raju [35]) is disclosed as

$$u\frac{\partial T}{\partial x} + v\frac{\partial T}{\partial y} = \frac{\kappa}{\rho C_p}\frac{\partial^2 T}{\partial y^2} + \frac{v}{C_p}(1-n)\left(\frac{\partial u}{\partial y}\right)^2 + \frac{vn\Gamma}{C_p\sqrt{2}}\frac{\partial u}{\partial y}\left(\frac{\partial u}{\partial y}\right)^2 + \frac{Q_0}{\rho C_p}(T - T_\infty) - \frac{1}{\rho C_p}\frac{\partial q_r}{\partial y}, \tag{25}$$

with boundary conditions

$$\left.\begin{aligned} T &= T_w \quad \text{at } y = 0; \\ T &= T_\infty \quad \text{as} y \longrightarrow \infty. \end{aligned}\right\} \tag{26}$$

Radiative heat flux amount q_r appears in equation (25). The radiative heat flux can be determined by thermal radiation adopting the Rosseland approximation, which is given by (Raptis (1998))

$$\begin{aligned} q_r \&9; &= -\frac{4\sigma^*}{3k^*}\frac{\partial T^4}{\partial y} \\ \&9; &= -\frac{16\sigma^*}{3k^*}\frac{\partial T}{\partial y}T_\infty{}^3. \end{aligned} \tag{27}$$

The dimensionless expression for temperature is

$$T = T_\infty + (T_w - T_\infty)\theta(\eta). \tag{28}$$

Using the relationships written in (16), (27), and (28), equation (25) becomes

$$(1+Nr)\theta'' + \mathrm{Pr}\left(S^*\theta' + Q\theta + (1-n)\mathrm{Ec}\left(f'\right)^2 + \frac{n}{2}\lambda_x Ec\left(f'\right)^3\right) = 0, \tag{29}$$

and reduced boundary constraints are

$$\left.\begin{aligned} \theta(\eta) &= 1 \quad \text{at } \eta = 0; \\ \theta(\eta) &\longrightarrow 0 \quad \text{as } \eta \longrightarrow \infty. \end{aligned}\right\} \tag{30}$$

In the above-mentioned model, all the applied non-dimensional parameters are defined as

$$\begin{aligned} \lambda_x &= \sqrt{2}\Gamma\frac{U_0 L}{x^2}\sqrt{\frac{U_0 L}{v}}, \\ \mathrm{Ha} &= \frac{\sigma {B_0}^2}{\rho}\frac{x^2}{U_0 L}, \\ \delta &= \frac{\mu}{\rho k_p}\frac{x^2}{U_0 L}, \\ Q &= \frac{Q_0 x^2}{\rho C_p U_0 L}, \\ \mathrm{Ec} &= \frac{{U_0}^2}{C_p(T_w - T_0)}, \\ \mathrm{Pr} &= \frac{\rho v C_p}{\kappa} \text{ and } \mathrm{Nr} = \frac{16\sigma^* T_\infty^3}{3k^*\kappa}. \end{aligned} \tag{31}$$

2.6. Skin Friction Coefficient and Heat Transfer Rate. From a practical standpoint, it is worthwhile to forecast the behaviour of the two physical parameters that are most helpful, namely wall friction and the Nusselt number.

$$\begin{aligned} C_{f_x} &= \frac{2\tau_w}{\rho U^2}, \\ \mathrm{Nu}_x &= \frac{x q_w}{\kappa(T_w - T_0)}, \end{aligned} \tag{32}$$

where $\tau_w = \mu[n\Gamma/\sqrt{2}\,(\partial u/\partial y)^2 + (1-n)\partial u/\partial y]$ (rate of shear stress) and $q_w = -\kappa(\partial T/\partial y) + (q_r)$ (energy flow/heat flux).

The dimensionless forms of all the physical quantities are described as

$$\begin{aligned} {\mathrm{Re}_x}^{1/2} C_{f_x} &= \left[(1-n)f' + \frac{n}{2}f'^2\lambda_x\right], \\ {Re_x}^{-1/2}\mathrm{Nu}_x &= -(1+\mathrm{Nr})\theta', \end{aligned} \tag{33}$$

where $\mathrm{Re}_x = U_0 L/v$ is local Reynold number.

3. Numerical Solution

The obtained dimensionless governing equations (17) and (29) are nonlinear in nature, and equation (29) is coupled due to the impact of momentum on the energy equation.

Here, MATLAB solver "Bvp4c" is used to get the answers to these couple of nonlinear second-order differential equations with boundary constraints (18) and (30). The Bvp4c method is a numerical method that can be utilised to resolve boundary value problems (BVPs) for ordinary differential equations (ODEs). The Bvp4c scheme employs a finite-difference approach with fourth-order precision. The flow process of Bvp4c is displayed in Figure 2.

The foregoing two equations (17) and (29) are translated into a set of differential equations of the first order to solve by "Bvp4c."

$$\left.\begin{aligned} f_1' &= f_2, \\ f_2' &= \frac{(1-f_1)^2 - S^* f_2 - (Ha+\delta)(1-f_1)}{(1-n)+\lambda_x n f_2}, \\ f_3' &= f_4, \\ f_4' &= -\frac{\Pr\left[S^* f_4 + (1-n)\mathrm{Ec}\, f_2^2 + n/2\lambda_x\, \mathrm{Ec}\, f_2^3 + Q f_3\right]}{(1+\mathrm{Nr})}, \end{aligned}\right\} \tag{34}$$

with

$$\left.\begin{aligned} f_1(0) &= 0, \quad f_3(0) = 1; \\ f_1(\infty) &= 1, \quad f_3(\infty) = 0. \end{aligned}\right\} \tag{35}$$

The acceptance error criterion is assumed in this case to be 10^{-4} with step size 0.01. To begin the computing procedure, the other two initial conditions $f_2(0)$ and $f_4(0)$ are believed to have reasonable approximations.

To assess the accuracy of obtained results via Bvp4c, we also solve the above system of equation (34) along with boundary conditions (35) using the RK-4 approach and find appropriate predication of initially absent conditions with standard and well-known shooting techniques. The results of these two numerical approaches are very comparable, as illustrated in Figures 3(a) and 3(b). Both the methods, Bvp4c and Runge–Kutta fourth order, can be used to solve a wide variety of ODEs, including those that are linear and nonlinear. Bvp4c can solve problems having singularities or discontinuity while the RK-4 approach has limitations.

4. Results and Discussion

The physical features of boundary layer emergence in the divergent porous channel of non-Newtonian tangent hyperbolic fluid flow with heat transfer in the appearance of a heat source and suction/blowing are examined in this analysis. The subsequent control parameters are taken to obtain the numerical solution: Weissenberg number $0 \le \lambda_x \le 0.5$, power law index $0 \le n \le 0.7$, mass suction $4 \le S^* \le 6$, Prandtl number $1 \le \Pr \le 4$, Eckert number $0 \le \mathrm{Ec} \le 1$, Hartmann number $0 \le \mathrm{Ha} \le 1$, porosity parameter $0 \le \delta \le 0.6$, heat source parameter $0 \le Q \le 2$, and radiation parameter $0.5 \le \mathrm{Nr} \le 1.5$. For the computational purpose, $n = 0.4$, $S^* = 4$, $\delta = 0.3$, $\lambda_x = 0.5$, $\Pr = 1$, $\mathrm{Ec} = 0.2$, $\mathrm{Ha} = 0.5$, $\mathrm{Nr} = 1$, and $Q = 2$ are fixed until stated separately. Numerical solutions are obtained by using the fourth-order exactness program (Bvp4c), and for validation of results, a comparison is also made with the fourth-order Runge–Kutta method in Figures 3(a) and 3(b). The outcomes of distinct physical parameters on flow characteristics (velocity and temperature) are visually investigated in Figures 4–9. Coefficient for skin friction and heat transfer rate profiles are also sketched visually in Figures 10 and 11. As indicated in Table 1, computed findings for skin friction drag coefficient and heat transfer rate are demonstrated for varying inputs of power law index parameter n.

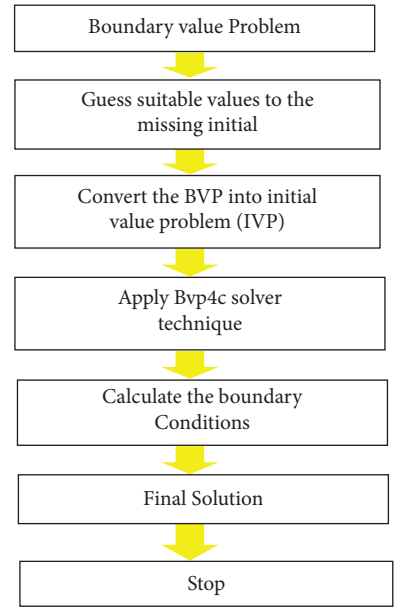

Figure 2: Flowchart of computational procedure.

4.1. Velocity and Temperature Profiles. Figures 4(a) and 4(b) depict the impact of the Weissenberg number λ_x on velocities and temperatures in the boundary layers, correspondingly. The Weissenberg number λ_x contrasts combined elastic and viscous forces. Typically, it is determined by the relationship between the time required for the fluid to relax under stress and the time required for a certain process. The rise in λ_x lengthens period for the fluid's stress relaxation, which rises the flow's opposition and, due to this, diminishes the velocity boundary layer. As λ_x increases, the width of the temperature boundary layer similarly raises as a consequence of these viscoelastic forces. The patterns not only of velocity but also of temperature for distinct inputs of the power law index n are sketched in Figures 5(a) and 5(b), correspondingly. The velocity increases together with enhancing inputs of n (as shown in Figure 5(a)) because the width of the boundary layer that develops close to the divergent channel wall reduces as n increases. In contrast, as n increases, the dimensionless profiles for temperature diminish. This is consistent with the info that the boundary layer's thickness increased as n rose. The consequences of external suction/blowing S^* on fluid velocity are seen in Figure 6(a). This demonstrates that the

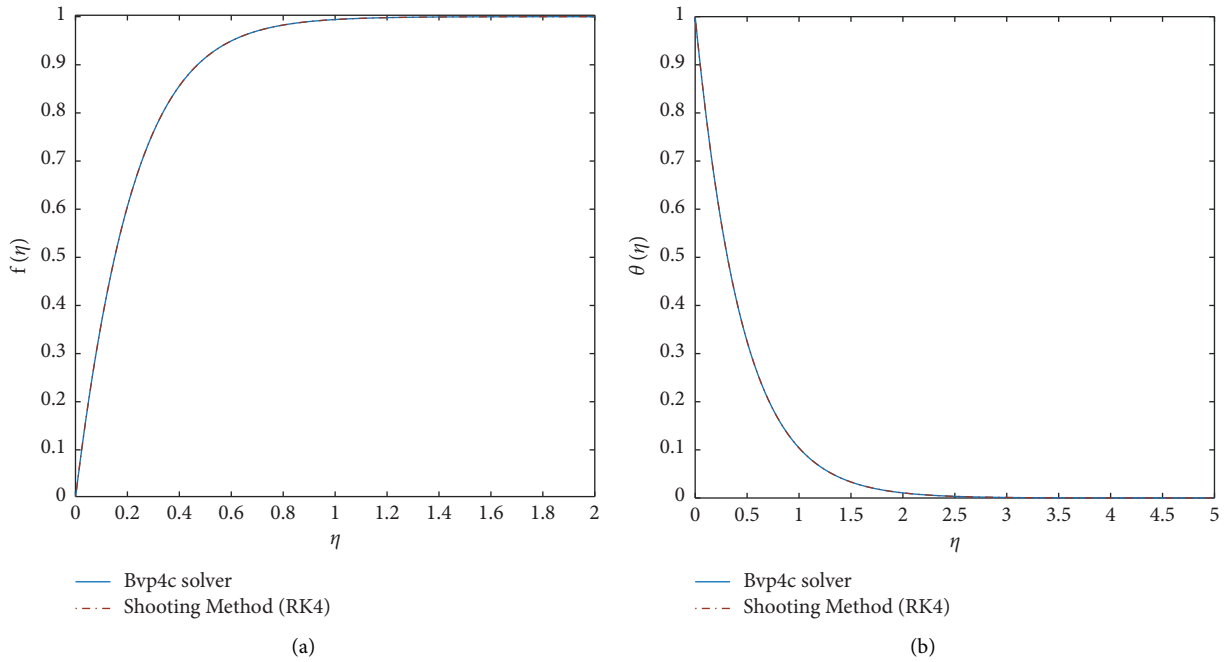

FIGURE 3: Comparison of momentum and temperature profiles obtained for $\lambda_x = 1$, Ec = 0.1, Pr = 1, Ha = 1, $\delta = 0.1$, Nr = 1, $Q = 1$, and $S^* = 5$ using "Bvp4c" and "Runge–Kutta fourth-order scheme."

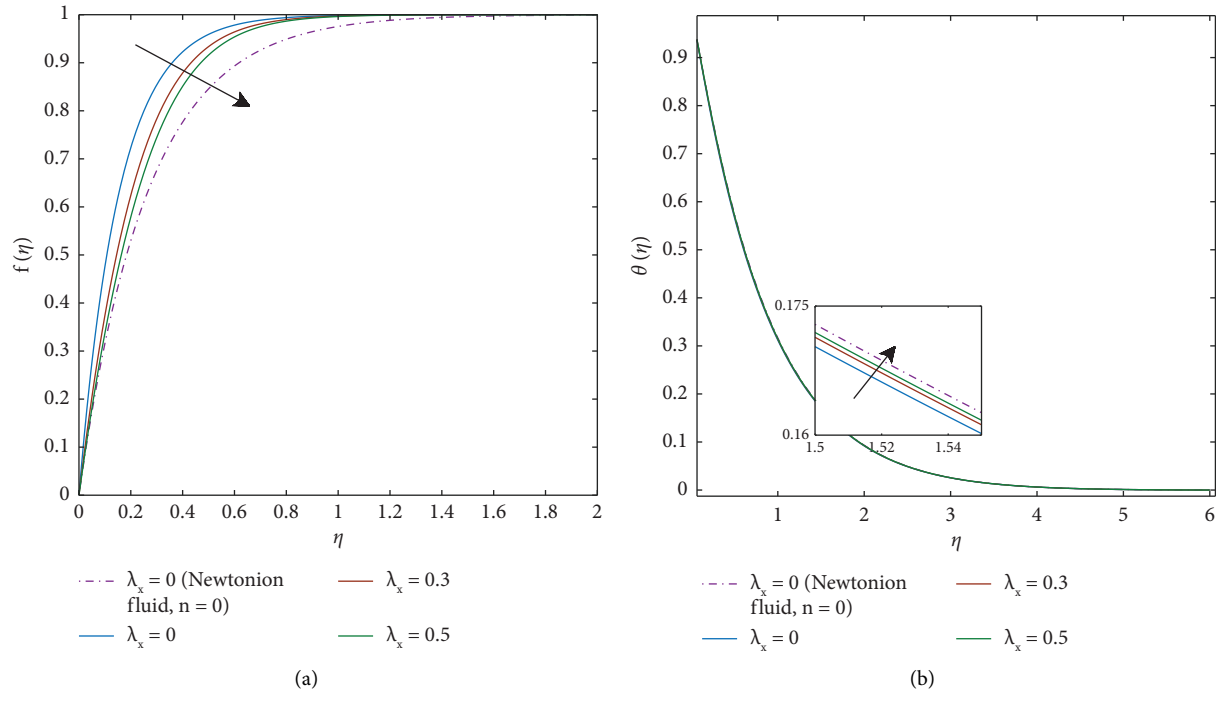

FIGURE 4: Momentum profile against λ_x (a) and temperature profile against λ_x (b).

boundary layer formation in the diverging channel is significantly influenced by the applied suction/blowing S^*. With an improvement in suction parameter S^*, the velocity rises. The thickness of the border layer is found to be reducing while Figure 6(b) illustrates how mass suction affects temperature. When the mass suction parameter is set to higher levels, the temperature profile falls. The low-temperature fluid is drawn in by mass suction closer to the wall, which lowers the temperature along the channel walls. Figures 7(a) and 7(b) depict the outcomes of Hartmann number Ha on velocity and temperature profiles. Growing inputs for Hartmann number Ha enhances the movement profile while declination is noticed for temperature profiles. Figure 8(a) depicts how the temperature is

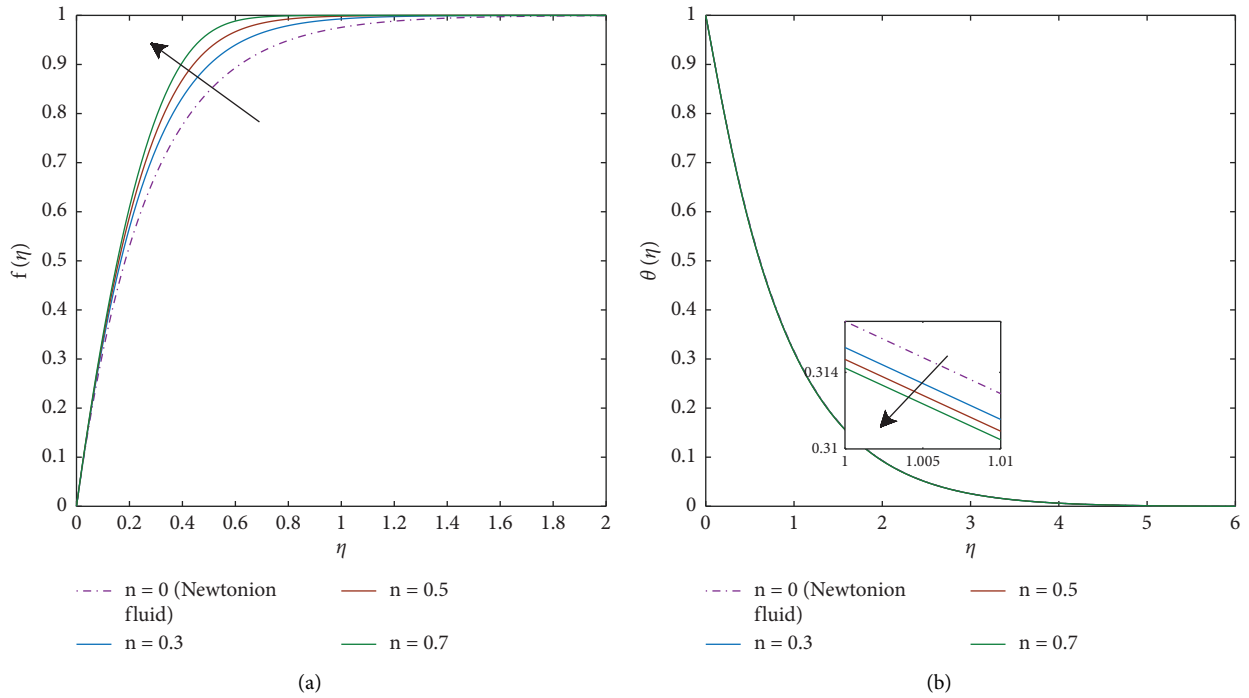

Figure 5: Momentum profile against n (a) and temperature profile against n (b).

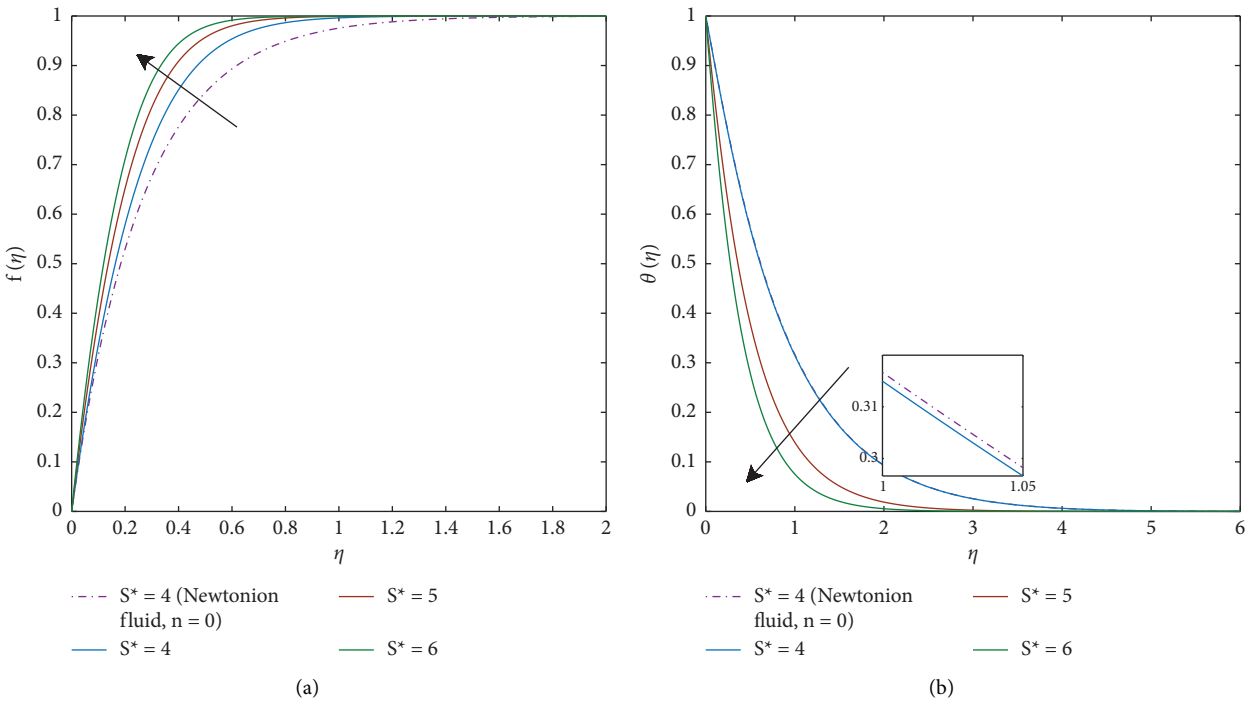

Figure 6: Momentum profile against S^* (a) and temperature profile against S^* (b).

influenced by the heat-generating parameter Q. This figure illustrates when the heat generation parameter Q is raised, there is an increase in both the overall temperature pattern and the width of the boundary layer since due to the presence of a heat source, heat is generated within the boundary layer, which regulates the temperature of the fluid to grow. The changes of the Eckert number Ec on the dimensionless temperature are set out in Figure 8(b). When the Eckert number Ec advances, the kinetic energy of the fluid is changed into internal energy through work versus the viscous fluid stresses. Due to this, increasing inputs of Ec, the temperature of the fluid is also enhanced. The resulting

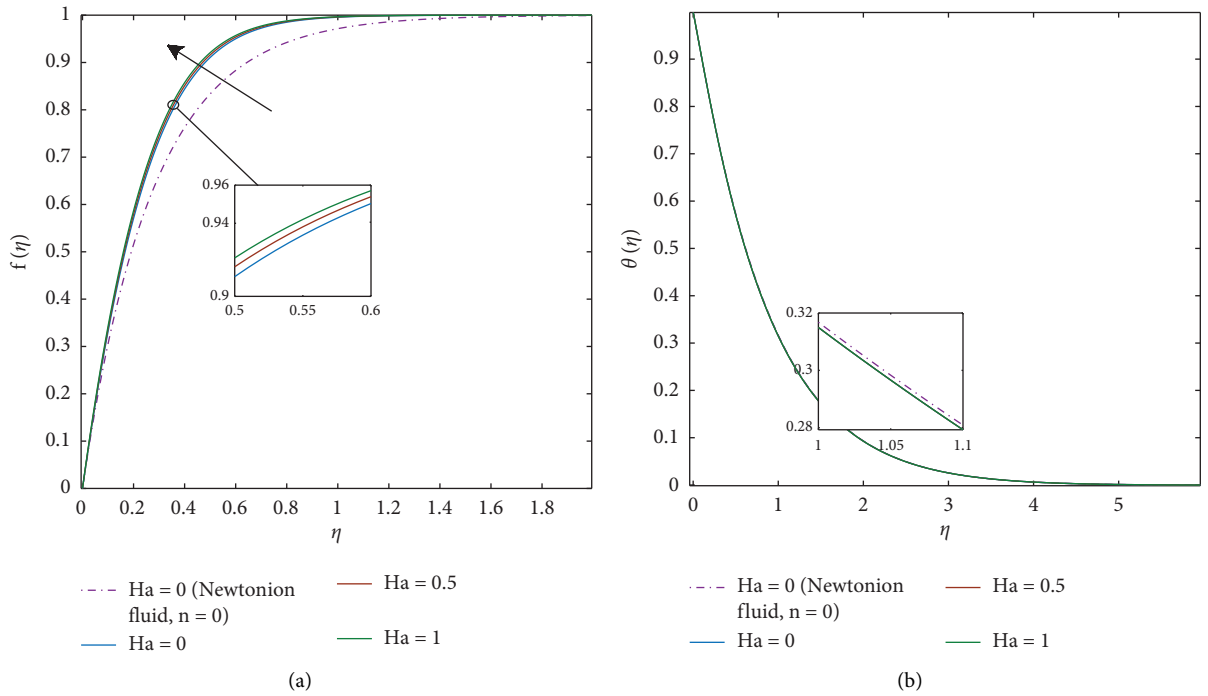

Figure 7: Momentum profile against Ha (a) and temperature profile against Ha (b).

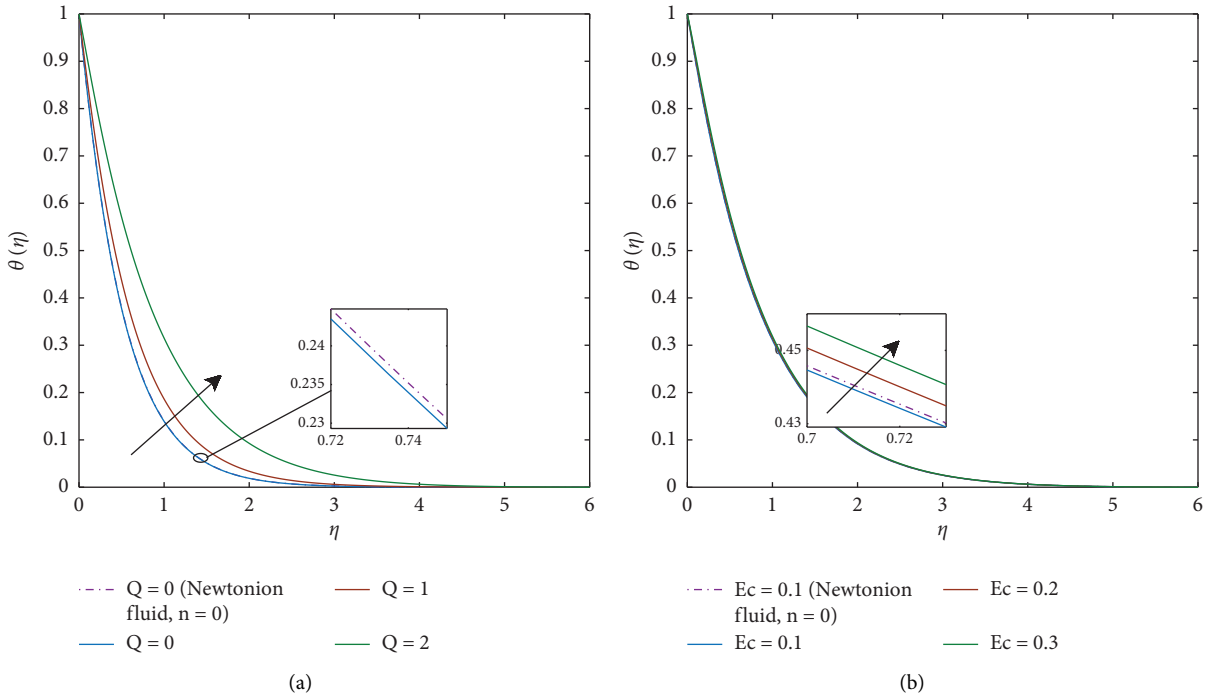

Figure 8: Temperature profiles against Q (a) and Ec (b).

consequences of radiation parameter Nr on the thermal boundary layer are displayed in Figure 9(a). The graph portrays that the temperature boundary layers grow as Nr increases. This outcome is anticipated because a source of heat is provided through thermal radiation and increases the amount of heat supplied to the flow. Figure 9(b) depicts the fluctuations in the correlation of nondimensional temperature with the Prandtl number Pr. It reveals that when Pr increases, the temperature decreases dramatically. As usual, a change is inversely proportional to fluid heat conductivity

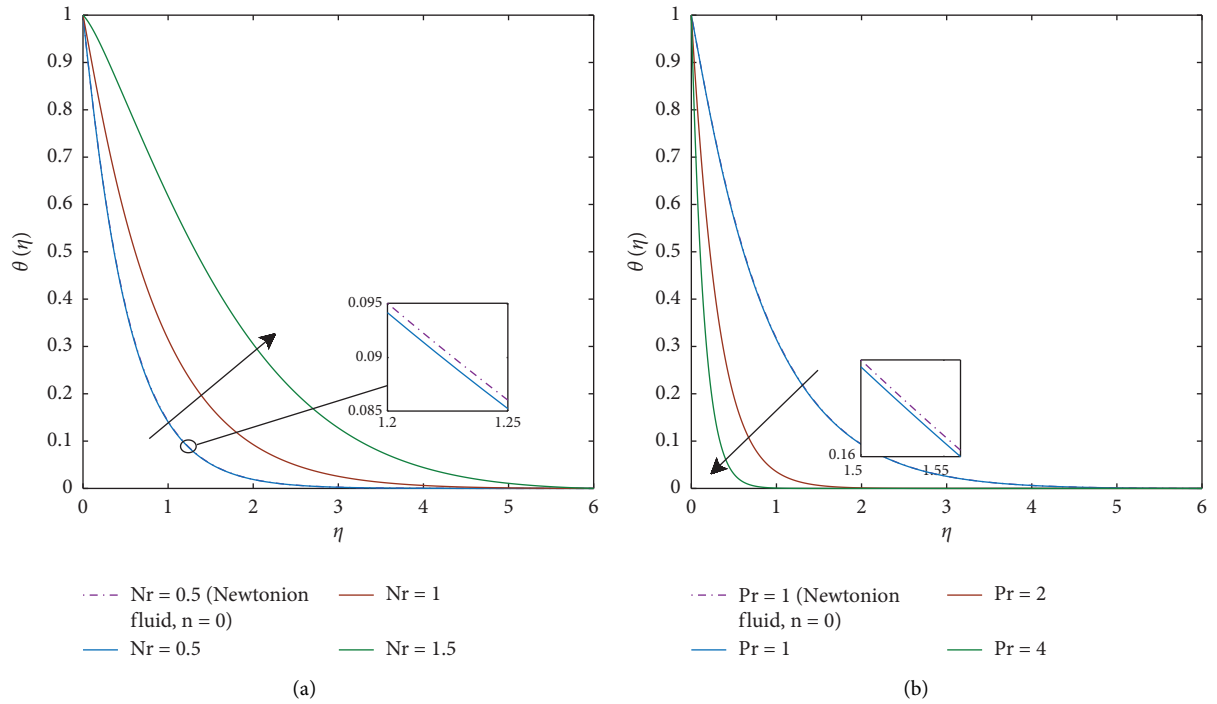

Figure 9: Temperature profiles against Nr (a) and Pr (b).

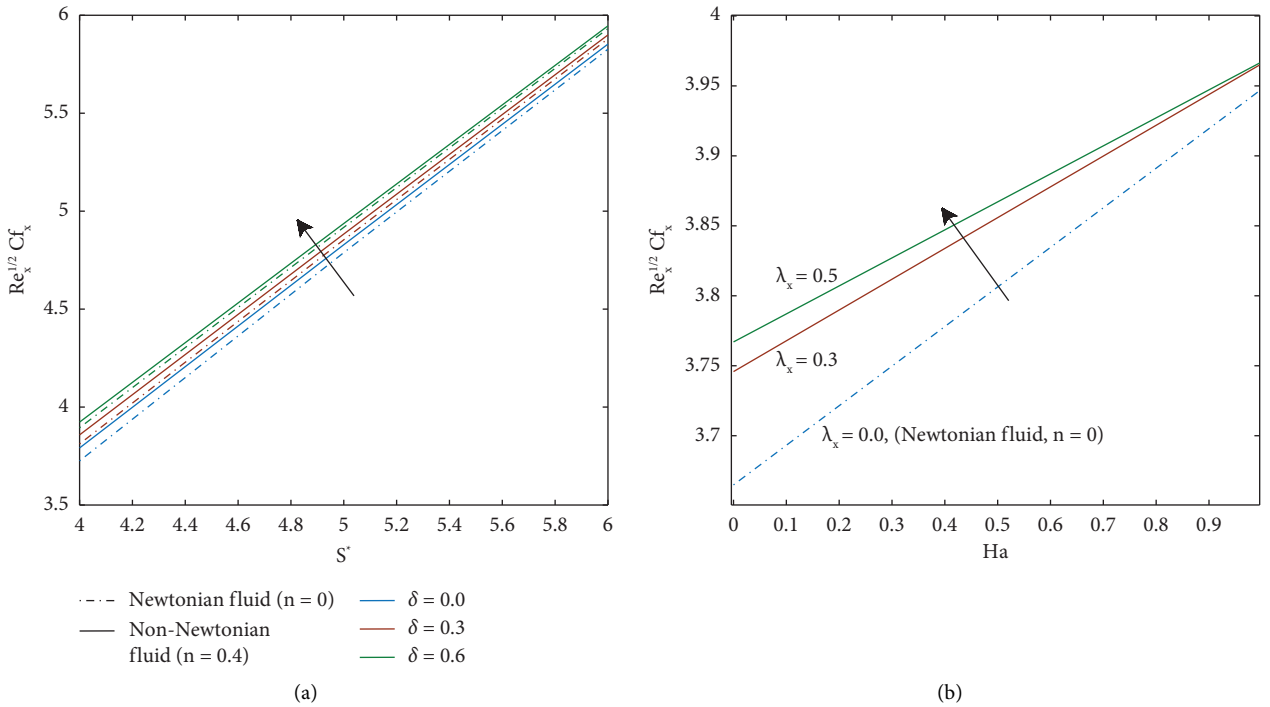

Figure 10: C_{f_x} influences in (a) and (b).

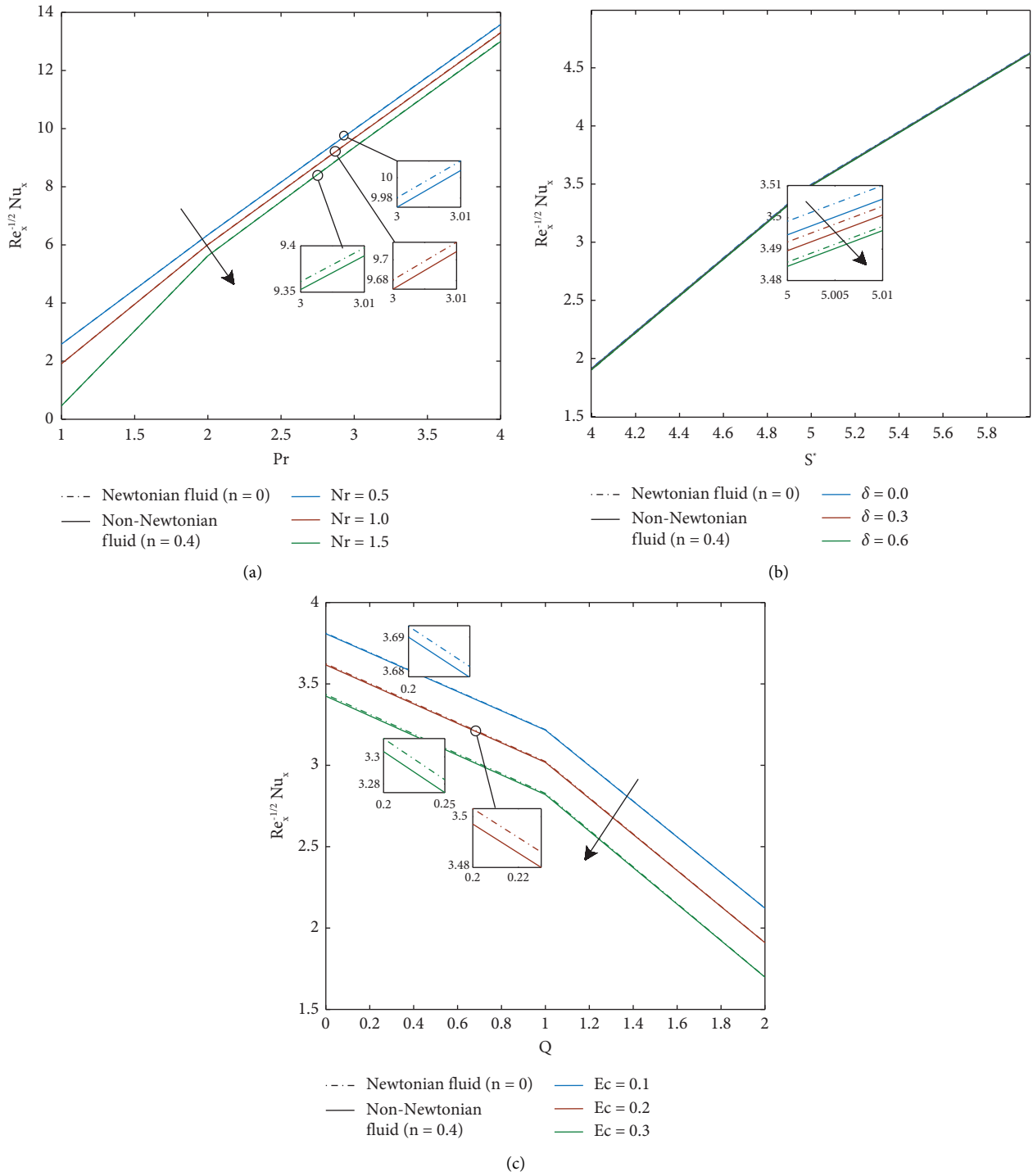

FIGURE 11: Nu_x influences in (a), (b), and (c).

κ, which means that as Pr increases, κ decreases. The temperature has dropped as a result of the aforementioned circumstance.

4.2. The Behaviour of Skin Friction Drag Coefficient, Heat Transfer Coefficient. Figures 10 and 11 correspondingly present the fluctuations of coefficient of skin friction $Re_x^{1/2} C_{f_x}$ and heat transfer rate $Re_x^{-1/2} Nu_x$ for the impacts of porosity parameter δ, Weissenberg number λ_x, radiation parameter Nr, and Eckert number Ec. From Figures 10(a) and 10(b), it is clear that with the growth in porosity parameter δ, suction parameter S^*, Hartmann number Ha, and Weissenberg number λ_x, skin-friction coefficient $Re_x^{1/2} C_{f_x}$ is discovered to be an increasing function. Heat transfer rate $Re_x^{-1/2} Nu_x$ decreases rapidly for rise inputs of radiation parameter Nr, porosity parameter δ, Eckert number Ec, and heat source parameter Q, which are shown in the

Table 1: Comparison of skin friction coefficient $\mathrm{Re}_x^{1/2}C_{f_x}$ and heat transfer rate $\mathrm{Re}_x^{-1/2}\mathrm{Nu}_x$ when $S^* = 5$, $\lambda_x = 1$, Ec = 0.1, Pr = 1, Ha = 1, $\delta = 0.1$, Nr = 1, and $Q = 1$.

S. no.	n	Present outcomes			
		Bvp4c		RK 4	
		$\mathrm{Re}_x^{1/2}C_{f_x}$	$\mathrm{Re}_x^{-1/2}\mathrm{Nu}_x$	$\mathrm{Re}_x^{1/2}C_{f_x}$	$\mathrm{Re}_x^{-1/2}\mathrm{Nu}_x$
1	0	4.9170	4.3112	4.9170	4.3112
2	0.1	4.9199	4.3112	4.9199	4.3112
3	0.3	4.9248	4.3104	4.9248	4.3104
4	0.5	4.9306	4.3096	4.9306	4.3096
5	0.6	4.9310	4.3094	4.9310	4.3094

Figures 11(a)–11(c) while enhanced behaviour is observed for Prandtl number Pr and suction parameter S^*.

From the above discussion, we are able to say that the skin-friction coefficient $\mathrm{Re}_x^{1/2}C_{f_x}$ profiles are rich in non-Newtonian fluids in comparison with those in Newtonian fluid ($n = 0$) while heat transfer rate $Re_x^{-1/2}Nu_x$ is low in non-Newtonian fluids in comparison with those in Newtonian fluids ($n = 0$).

5. Conclusions

The following major observations may be drawn from the preceding study of tangent hyperbolic fluid flow and heat transfer with a heat source and suction/blowing phenomenon in a divergent channel:

(a) A sufficient quantity of mass suction ($S^* \geq 2\sqrt{[2-(Ha+\delta)](1-n)}$) is required for the emergence of hyperbolic tangent fluid boundary layer flow.

(b) Weissenberg number λ_x causes a decrease in velocity while increasing λ_x causes just a very small improvement in temperature magnitudes. Also, an opposite scenario is noticed for the power law index n.

(c) Whenever thermal radiation Nr introduces more heat into the fluid, intensifying the temperature and thickness of its boundary layer, the temperature distribution is stronger in the occurrence of thermal radiation. Due to the availability of internal heat source Q, the energy is released, so the temperature profile also increases.

(d) Both radiation parameter Nr and heat source parameter Q have declined profile for Nusselt number.

(e) The skin friction coefficient $\mathrm{Re}_x^{1/2}C_{f_x}$ is a boosting function of the suction parameter S^*, Hartmann number Ha, local Weissenberg number λ_x, porosity parameter δ, and power law index n.

The present problem can be discussed for other non-Newtonian fluids such as Maxwell fluid, Jeffrey fluid, and Williamson fluid, considering different boundary conditions. Behaviour of bioconvection, Cattaneo–Christov heat flux, and entropy generation can be explored for the present problem.

Nomenclature

$\overleftrightarrow{M}$: Cauchy stress tensor ($\mathrm{N/m^2}$)
C_p: Capacity of heat at constant pressure (J/K)
Ha: Hartmann number
$\overrightarrow{B}$: Body force ($\mathrm{kg{\cdot}m/s^2}$)
$f(\eta)$: Dimensionless fluid velocity
I: Identity tensor
k_p: Permeability of the medium (m^2)
L: Characteristic length (m)
n: Power law index
p: Pressure ($\mathrm{N/m^2}$)
Pr: Prandtl number
Q_0: A positive constant
Re: Local Reynold number
k^*: Mean absorption coefficient
x, y: Cartesian coordinates (m)
T_0: Reference temperature (K)
S^*: Mass suction/blowing parameter
u, v: Velocity components (m/s)
U_0: Reference velocity (m/s)
$\overrightarrow{V} = (u, v)$: Velocity vector (m/s)
Q: Parameter for heat generation/absorption
Nr: Radiation parameter

Greek Symbols

μ: Dynamic viscosity (kg/m s)
μ_∞: Infinite shear rate viscosity (kg/m s)
τ: Extra stress tensor ($\mathrm{N/m^2}$)
ρ: Fluid density ($\mathrm{kg/m^3}$)
σ: Fluid electrical conductivity ($\mathrm{K^3A^2/kg{\cdot}m^3}$)
$\theta(\eta)$: Fluid temperature (K)
υ: Kinematic viscosity ($\mathrm{m^2/s}$)
δ: Porosity parameter
μ_0: Zero shear rate viscosity (kg/m s)
χ: Second invariant strain tensor $\mathrm{s^{-2}}$
$\dot{\gamma}$: Shear rate ($\mathrm{s^{-1}}$)
τ_w: Shear stress ($\mathrm{N/m^2}$)
η: Similarity variable
ψ: Stream function
λ_x: Local Weissenberg number
$\Gamma > 0$: Time-dependent material constant (s)
κ: Thermal conductivity (W/m·K)
α: Channel angle
σ^*: Stefan–Boltzmann constant.

Data Availability

The raw data supporting the conclusions of this article will be made available by the corresponding author without undue reservation.

Conflicts of Interest

The authors declare that they have no conflicts of interest.

References

[1] I. Pop and D. B. Ingham, *Convective Heat Transfer: Mathematical and Computational Modelling of Viscous Fluids and Porous media*, Elsevier Science, Amsterdam, Netherlands, 2001.

[2] E. Brujan, *Cavitation in Non-newtonian Fluids: Biomedical and Bioengineering Applications*, Springer Science & Business Media, Heidelberg, Germany, 2010.

[3] N. S. Akbar, S. Nadeem, R. U. Haq, and Z. H. Khan, "Numerical solution of MHD boundary layer flow of tangent hyperbolic fluid towards a stretching sheet," *Indian Journal of Physics*, vol. 87, no. 11, pp. 1121–1124, 2013.

[4] V. R. Prasad, S. A. Gaffar, E. K. Reddy, and O. A. Beg, "Free convection flow and heat transfer of non-Newtonian tangent hyperbolic fluid from an isothermal sphere with partial slip," *Arabian Journal for Science and Engineering*, vol. 39, no. 11, pp. 8157–8174, 2014.

[5] V. Ramachandra Prasad, S. Abdul gaffar, E. Kesava Reddy, and O. A. Beg, "Computational Analysis of magnetohydrodynamic free convection flow and heat transfer of non-Newtonian tangent hyperbolic fluid forms a horizontal circular cylinder with partial slip," *International Journal of Algorithms, Computing and Mathematics*, vol. 4, pp. 651–675, 2015.

[6] M. A. Abbas, Y. Q. Bai, M. M. Bhatti, and M. M. Rashidi, "Three-dimensional peristaltic flow of hyperbolic tangent fluid in nonuniform channel having flexible walls," *Alexandria Engineering Journal*, vol. 55, no. 1, pp. 653–662, 2016.

[7] S. Farooq, M. I. Khan, T. Hayat, M. Waqas, and A. Alsaedi, "Theoretical investigation of peristalsis transport in flow of hyperbolic tangent fluid with slip effects and chemical reaction," *Journal of Molecular Liquids*, vol. 285, p. 314-322, 2019.

[8] S. Sindhu and B. J. Gireesha, "Heat and mass transfer analysis of chemically reactive tangent hyperbolic fluid in a microchannel," *Heat Transfer*, vol. 50, no. 2, pp. 1410–1427, 2021.

[9] S. Ahmad, R. D. Khan, and S. Zeb, "Lie group analysis of hyperbolic tangent fluid flow in the presence of thermal radiation," *Heat Transfer*, vol. 51, no. 4, pp. 3067–3081, 2022.

[10] K. Jat and K. Sharma, "Unsteady MHD flow of tangent hyperbolic nanofluid over an inclined stretching sheet and heat transfer analysis," *NanoWorld J*, vol. 8, no. S1, pp. S104–S110, 2022.

[11] F. Ali, K. Loganathan, S. Eswaramoorthi, M. Faizan, E. Prabu, and A. Zaib, "Bioconvective applications of unsteady slip flow over a tangent hyperbolic nanoliquid with surface heating: improving energy system performance," *International Journal of Algorithms, Computing and Mathematics*, vol. 8, no. 6, p. 276, 2022.

[12] A. U. Yahya, I. Siddique, N. Salamat, S. Abdal, and S. Hussain, "A numerical investigation for tangent hyperbolic hybrid nanofluid transportation across Riga wedge," *Waves in Random and Complex Media*, pp. 1–13, 2022.

[13] G. B. Jeffery, "L. The two-dimensional steady motion of a viscous fluid," *The London, Edinburgh and Dublin Philosophical Magazine and Journal of Science*, vol. 29, no. 172, pp. 455–465, 1915.

[14] G. Hamel, *Spiralförmige Bewegungen zäher Flüssigkeiten. Jahresbericht der deutschen mathematiker-vereinigung*, vol. 25, pp. 34–60, 1917.

[15] P. E. Haines, R. E. Hewitt, and A. L. Hazel, "The Jeffery–Hamel similarity solution and its relation to flow in a diverging channel," *Journal of Fluid Mechanics*, vol. 687, pp. 404–430, 2011.

[16] K. Bhattacharyya and G. C. Layek, "MHD boundary layer flow of dilatant fluid in a divergent channel with suction or blowing," *Chinese Physics Letters*, vol. 28, no. 8, Article ID 084705, 2011.

[17] G. C. Layek, S. G. Kryzhevich, A. S. Gupta, and M. Reza, "Steady magnetohydrodynamic flow in a diverging channel with suction or blowing," *Zeitschrift für Angewandte Mathematik und Physik*, vol. 64, pp. 123–143, 2013.

[18] M. T. Erdinç, "Numerical investigation of flow and heat transfer in communicating converging and diverging channels," *Journal of Thermal Engineering*, vol. 4, no. 5, pp. 2318–2332, 2018.

[19] I. Iyyappan and A. K. Singh, "MHD flows on irregular boundary over a diverging channel with viscous dissipation effect," *International Journal of Numerical Methods for Heat and Fluid Flow*, vol. 31, no. 7, pp. 2112–2127, 2021.

[20] A. Banerjee, S. K. Mahato, K. Bhattacharyya, and A. J. Chamkha, "Divergent channel flow of Casson fluid and heat transfer with suction/blowing and viscous dissipation: existence of boundary layer," *Partial Differential Equations in Applied Mathematics*, vol. 4, Article ID 100172, 2021.

[21] I. Siddique, K. Sadiq, F. Jarad, M. K. Al Mesfer, M. Danish, and S. Yaqoob, "Analysis of natural convection in nanofluid flow through a channel with source/sink effect," *Journal of Nanomaterials*, vol. 2022, Article ID 2738398, 9 pages, 2022.

[22] A. M. Alqahtani, M. R. Khan, N. Akkurt, V. Puneeth, A. Alhowaity, and H. Hamam, "Thermal analysis of a radiative nanofluid over a stretching/shrinking cylinder with viscous dissipation," *Chemical Physics Letters*, vol. 808, Article ID 140133, 2022.

[23] D. Qaiser, Z. Zheng, M. Riaz Khan, and A. M. Galal, "Significance of activation energy and entropy optimization in radiative stagnation point flow of nanofluid with cross-diffusion and viscous dissipation," *Waves in Random and Complex Media*, pp. 1–22, 2022.

[24] M. R. Khan, N. A. Ahammad, S. E. Alhazmi et al., "Energy and mass transport through hybrid nanofluid flow passing over an extended cylinder with the magnetic dipole using a computational approach," *Frontiers in Energy Research*, vol. 10, 2022.

[25] M. Faisal, K. K. Asogwa, N. Alessa, and K. Loganathan, "Nonlinear radiative nanofluidic hydrothermal unsteady bidirectional transport with thermal/mass convection aspects," *Symmetry*, vol. 14, no. 12, p. 2609, 2022.

[26] R. Prabakaran, S. Eswaramoorthi, K. Loganathan, and S. Gyeltshen, "Thermal radiation and viscous dissipation impacts of water and kerosene-based carbon nanotubes over a heated Riga sheet," *Journal of Nanomaterials*, vol. 2022, Article ID 1865763, 17 pages, 2022.

[27] L. Rundora and O. D. Makinde, "Effects of suction/injection on unsteady reactive variable viscosity non-Newtonian fluid flow in a channel filled with porous medium and convective boundary conditions," *Journal of Petroleum Science and Engineering*, vol. 108, pp. 328–335, 2013.

[28] S. Mansur, A. Ishak, and I. Pop, "The magnetohydrodynamic stagnation point flow of a nanofluid over a stretching/shrinking sheet with suction," *Public Library of Science One*, vol. 10, no. 3, Article ID e0117733, 2015.

[29] I. L. Animasaun, E. A. Adebile, and A. I. Fagbade, "Casson fluid flow with variable thermo-physical property along exponentially stretching sheet with suction and exponentially decaying internal heat generation using the homotopy analysis method," *Journal of the Nigerian Mathematical Society*, vol. 35, no. 1, pp. 1–17, 2016.

[30] A. Hussanan, M. Z. Salleh, I. Khan, and S. Shafie, "Analytical solution for suction and injection flow of a viscoplastic Casson fluid past a stretching surface in the presence of viscous dissipation," *Neural Computing & Applications*, vol. 29, no. 12, pp. 1507–1515, 2018.

[31] B. Li, Y. Yang, and X. Chen, "A power-law liquid food flowing through an uneven channel with non-uniform suction/injection," *International Journal of Heat and Mass Transfer*, vol. 144, Article ID 118639, 2019.

[32] S. Abdal, S. Hussain, I. Siddique, A. Ahmadian, and M. Ferrara, "On solution existence of MHD Casson nanofluid transportation across an extending cylinder through porous media and evaluation of priori bounds," *Scientific Reports*, vol. 11, no. 1, p. 7799, 2021.

[33] Z. Asghar, R. S. Saif, and N. Ali, "Investigation of boundary stresses on MHD flow in a convergent/divergent channel: an analytical and numerical study," *Alexandria Engineering Journal*, vol. 61, no. 6, pp. 4479–4490, 2022.

[34] J. L. Bansal, *Viscous Fluid Dynamics*, Jaipur Publication House, Jaipur, India, 2008.

[35] M. Patil and C. S. K. Raju, "Convective conditions and dissipation on Tangent Hyperbolic fluid over a chemically heating exponentially porous sheet," *Nonlinear Engineering*, vol. 8, no. 1, pp. 407–418, 2019.